Inorganic Chemistry

Article

pubs.acs.org/IC

Measured and Calculated Oxidation Potentials of 1-X-12-Y-$CB_{11}Me_{10}^-$ Anions

Abdul Wahab,[†,‡] Brian Stepp,[‡,§] Christos Douvris,[§] Michal Valášek,[‡] Jan Šturse,[‡] Jiří Klíma,[†] Mari-Carmen Piqueras,[∥] Raül Crespo,[∥] Jiří Ludvík,*[,†] and Josef Michl*[,‡,§]

[†]J. Heyrovský Institute of Physical Chemistry, Academy of Sciences of the Czech Republic, Dolejškova 3, 18223 Prague 8, Czech Republic

[‡]Institute of Organic Chemistry and Biochemistry, Academy of Sciences of the Czech Republic, Flemingovo nám. 2, 16610 Prague 6, Czech Republic

[§]Department of Chemistry and Biochemistry, University of Colorado, Boulder, Colorado 80309-0215, United States

[∥]Departament de Química Física, Universitat de València, Dr. Moliner 50, E-46100 Burjassot, Spain

Supporting Information

ABSTRACT: Cyclic voltammetry of 31 icosahedral carborane anions 1-X-12-Y-$CB_{11}Me_{10}^-$ at a Pt electrode in liquid SO_2 revealed a completely reversible one-electron oxidation even at low scan rates, except for the anions with Y = I, which are oxidized irreversibly up to a scan rate of 5.0 V/s, and the anion with X = COOH and Y = H, whose oxidation is irreversible at scan rates below 1.0 V/s. Relative reversible oxidation potentials agree well with RI-B3LYP/TZVPP,COSMO and significantly less well with RI-BP86/TZVPP,COSMO or RI-HF/TZVPP,COSMO calculated adiabatic electron detachment energies. Correlations with HOMO energies of the anions are nearly as good, even though the oxidized forms are subject to considerable Jahn−Teller distortion. Except for the anion with X = F and Y = Me, the oxidation potentials vary linearly with substituent σ_p Hammett constants. The slopes (reaction constants) are ∼0.31 and ∼0.55 V for positions 1 and 12, respectively.

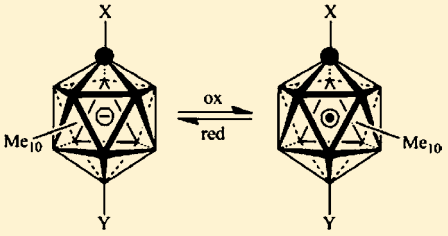

INTRODUCTION

Unlike most weakly nucleophilic anions, those derived from the three dimensionally aromatic[1] icosahedral $CB_{11}H_{12}^-$ anion[2] (Figure 1) offer the prospect of great stability for both members of the redox pair, anion and radical, and this could make them useful as redox shuttles in photovoltaic cells. Anions derived from $CB_{11}H_{12}^-$ have also found other applications: as counterions for highly reactive cations,[3] including organometallic catalysts[4] and "naked" lithium cations, capable of catalyzing radical polymerization of simple alkenes,[5−7] as electrolytes for unusual nonaqueous solvents such as silicone oil[8] and for electrical batteries,[9] as solubilizers of cations in organic solvents,[10] for instance in solvent extraction of radionuclides,[11] etc. The radicals have been used as unusually strong[12] neutral oxidants soluble in organic solvents.[13]

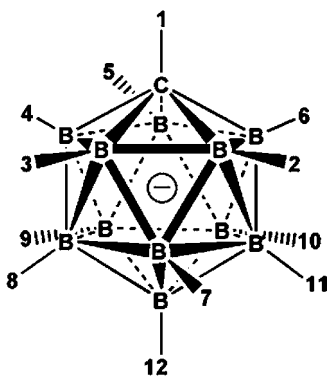

Figure 1. Vertex numbering in the CB_{11} icosahedron.

Full reversibility of the oxidation−reduction process is an important goal. It is unlikely that the as yet unobserved oxidation of the parent $CB_{11}H_{12}^-$ could be reversible. The easier[14] oxidation of the analogous unsubstituted anions $CB_9H_{10}^-$,[15] $B_{10}H_{10}^{2-}$,[16−18] and $B_{12}H_{12}^{2-}$[19] is not, because the radical dimerizes to a hypercloso species with a deprotonated ("naked") boron vertex, and the parent $CB_{11}H_{12}^{\bullet}$ will probably do the same. However, there are promising indications that a suitable choice of sterically encumbering substituents will prevent such dimerization. The permethylated anion **1** and four others of the 15 possible symmetrically methylated anions, all heavily substituted in the hemisphere antipodal to the carbon vertex (positions 7−12, Figure 1), give reversible peaks in liquid SO_2, and it appears that substitution at these positions is important for preventing radical dimerization. The radical $CB_{11}Me_{12}^{\bullet}$ has been isolated and characterized by X-ray diffraction,[13] and certain radicals carrying F and CF_3 substituents also appear to be resistant to dimerization.[12]

Received: December 14, 2011
Published: April 18, 2012

   dx.doi.org/10.1021/ic2026939 | *Inorg. Chem.* 2012, 51, 5128−5137

Table 1. Anodic Oxidation Potentials ($E_{1/2}$ or E_{pa}, V vs Fc/Fc^+) of $Cs[1\text{-}X\text{-}12\text{-}Y\text{-}(2\text{-}11)\text{-}Me_{10}CB_{11}]$ in Liquid SO_2 at 0.2 V/s

			obsd		B3LYP			BP86		HF	
no.	X	Y	ΔE_p [a]	$E_{1/2}$ [b]	$E_{1/2}^{\Delta E}$ [c]	$E^*_{1/2}{}^{\Delta E}$ [d]	$-E^{aHOMO}$ [e]	$E_{1/2}^{\Delta E}$ [f]	$-E^{aHOMO}$ [g]	$E_{1/2}^{\Delta E}$ [h]	$-E^{aHOMO}$ [i]
1	CH_3	CH_3	48	1.16	(1.16)		5.98	(1.16)	5.35	(1.16)	8.26
2	H	CH_3	49	1.19	1.18		5.99	1.18	5.38	1.20	8.28
3[j]	C_2H_5	CH_3	48	1.16							
4	C_3H_7	CH_3	51	1.17							
5	OCH_3	CH_3	48	1.20	1.19		6.00	1.12	5.25	1.29	8.31
6	C_4H_9	CH_3	47	1.16							
7[k]	C_6H_{13}	CH_3	53	1.20							
8	$B(OH)_2$	CH_3	56	1.32	1.32		6.14	1.32	5.51	1.31	8.43
9	F	CH_3	51	1.34	1.34		6.16	1.33	5.53	1.39	8.47
10	Br	CH_3	54	1.31	1.35		6.18	1.34	5.57	1.39	8.50
11	I	CH_3	52	1.31	1.34		6.18	1.31	5.56	1.37	8.49
12	COOH	CH_3	55	1.32	1.34		6.16	1.34	5.63	1.36	8.45
13	$COOCH_3$	CH_3	54	1.35	1.31		6.13	1.29	5.50	1.33	8.43
14	H	H	56	1.26	1.23		6.08	1.24	5.45	1.25	8.32
15	CH_3	H	54	1.23	1.21		6.03	1.21	5.41	1.23	8.31
16	C_2H_5	H	53	1.24							
17	C_4H_9	H	51	1.24							
18	C_6H_{13}	H	52	1.23							
19	$CH_2CH(C_2H_5)C_4H_9$	H	54	1.22							
20	COOH	H	70	1.40	1.38		6.21	1.40	5.68	1.41	8.50
21	H	F	58	1.34	1.31		6.12	1.27	5.47	1.34	8.43
22	CH_3	F	49	1.31	1.29		6.11	1.25	5.47	1.32	8.42
23	H	Cl	61	1.39	1.39		6.19	1.36	5.56	1.45	8.51
24	H	Br	57	1.42	1.41		6.24	1.37	5.59	1.49	8.55
25	H	I	irr	(1.43)	1.40	1.40	6.12	1.32	5.45	1.51	8.58
26	CH_3	I	irr	(1.39)	1.38	1.38	6.11	1.30	5.47	1.49	8.57
27	C_2H_5	I	irr	(1.40)							
28[l]	C_3H_7	I	irr	(1.41)							
29	C_4H_9	I	irr	(1.38)							
30	C_6H_{13}	I	irr	(1.39)							
31	$COOCH_3$	I	irr	(1.52)	1.49	1.48	6.19	1.39	5.55	1.64	8.72

[a]Peak separation potentials in mV. [b]$E_{1/2} = (E_{pa} - E_{pc})/2 = \Delta E_p/2$; irreversible oxidation potentials (in parentheses) are represented by E_{pa}. [c]Calculated (RI-DFTB3LYP/TZVPP,COSMO) adiabatic electron detachment energy ΔE of the anion in solvent with respect to Fc/Fc^+, relative to the value observed for **1** (4.57 eV subtracted from the absolute value). [d]Redox potential derived from the best regression line for state energy difference calculation: $E_{1/2}{}^{\Delta E} = 0.92\Delta E + 0.11$ (V). [e]Anion HOMO energy (RI-DFTB3LYP/TZVPP,COSMO). [f]Calculated (RI-DFTBP86/TZVPP,COSMO) adiabatic electron detachment energy ΔE of the anion in solvent with respect to Fc/Fc^+, relative to the value observed for **1** (4.53 eV subtracted from the absolute value). [g]Anion HOMO energy (RI-DFTBP86/TZVPP,COSMO). [h]Calculated (RI-HF/TZVPP,COSMO) adiabatic electron detachment energy ΔE of the anion in solvent with respect to Fc/Fc^+, relative to the value observed for **1** (4.04 eV subtracted from the absolute value). [i]Anion HOMO energy (RI-HF/TZVPP,COSMO). [j]Cation: Ph_4P^+. [k]Cation: Me_3NH^+. [l]Cation: Me_4N^+.

Anions derived from $CB_{11}H_{12}^-$ by introduction of substituents generally have very high oxidation potentials. The parent does not give a clear cyclic voltammetric peak in acetonitrile[15] or in liquid SO_2,[20] and those carrying several $-F$ and $-CF_3$ substituents are not oxidized even with the strongest known chemical oxidation agents, such as the salts of O_2^+ or NiF_3^+ (their calculated gas-phase electron detachment energies are as high as 8 eV).[12,21] This behavior is reminiscent of other "inoxidizable" anions such as BF_4^-, PF_6^-, and AsF_6^- and contrasts with that of more common boron-based anions such as BPh_4^-, $B_{12}H_{12}^{2-}$, and $B(C_6F_5)_4^-$, known to undergo irreversible oxidation at 0.56,[22] 1.02,[19] and 2.1 V[23] against the ferrocene/ferrocenium (Fc/Fc^+) standard, respectively. Even the redox potential of the electron-rich dodecamethylated anion **1** relative to Fc/Fc^+, although much lower than that of the parent $CB_{11}H_{12}^-$,[20] has been reported to be as high as 1.16 V in acetonitrile[24] and 1.08 V in liquid SO_2.[20] Methyl substitution alone thus allows the *closo*-monocarbadodecaborane anions to span a respectable redox potential range of at least 1.5 V. Methyl is believed to act by hyperconjugative electron density donation, as the local symmetry of the two highest doubly degenerate occupied molecular orbitals of the anion, HOMO and HOMO-1,[20] is suitable for interaction with π-symmetry orbitals of substituents, likely making the redox potential sensitive to the π-electron effect of substituents. Methyl is a net electron withdrawer on boron in an absolute sense,[25] presumably due to its σ-electron effect, but it clearly is a π donor relative to the hydrogen substituent standard. The effects of multiple methyl substituents are additive, and each inequivalent cage position has been characterized by an increment characterizing its sensitivity to methyl substitution (52, 68, 70, and 9 mV for positions 1, 2, 7, and 12, respectively[20]). For many of the intended applications the redox potential needs to be adjustable to a particular value, and given the availability of 12 substitution positions in $CB_{11}H_{12}^-$, it is likely that with a wider variety of substituents fine-tuning of the redox potential will be possible across a very wide range.

dx.doi.org/10.1021/ic2026939 | Inorg. Chem. 2012, 51, 5128−5137

We have embarked on a program of synthesis,[20,26,27] electrochemical,[20] and quantum-chemical[20] characterization of a large number of substituted $CB_{11}H_{12}^-$ anions in the hope of identifying those most suitable for photovoltaic and similar applications in terms of both the stability of the oxidized and reduced forms and the redox potential value. Presently, we report results for 31 substituted derivatives, with focus on the effect of substitution in the axial positions 1 and 12 (**1**−**31**, Table 1). Most of the anions were known,[26,27] and two (**23** and **24**) were newly synthesized for the purpose. In order to maximize the probability that the oxidation in liquid SO_2 will be reversible, boron vertices 2−11 in **1**−**31** always carried methyl substituents, while the substituents at positions 1 and 12 were varied. This strategy paid off in that most choices of substituents produced fully chemically reversible oxidation behavior. A study of the effect of substituent variation in positions 2−11 is also needed but will have to await further synthetic advances.

In comparison with the initial investigation of methylated $CB_{11}H_{12}^-$ anions,[20] the present data provide a considerably improved testing ground for an evaluation of the performance of quantum theory for the prediction of electrochemical redox potentials for anodic oxidation. The availability of reversible potentials measured for 24 related anions with very similar sizes and shapes (and therefore, also solvent cavities) is unusual. Moreover, the degeneracy and near-degeneracy of up to four of their highest occupied molecular orbitals (HOMOs), which causes first- and second-order Jahn−Teller distortions in the neutral radicals,[20] poses a particular challenge to theory. We note that there have been many prior successful reports that account for observed electrochemical redox potentials of a series of related substrates using quantum chemical methods,[28,29] and we cite several representative examples: transition-metal ions,[30−34] small organic molecules,[35] anilines,[36] nitroaromatics,[37] organometallic complexes,[38−40] methylated carborane anions,[20] organic radicals,[41] diketones,[42] and carbamates.[43] We now compare the performance of two popular DFT functionals and the Hartree−Fock method.

RESULTS

The electrochemical oxidation of Cs salts of the carborane anions was studied by cyclic voltammetry at a Pt electrode at −65 °C in liquid SO_2, which dissolves all the salts well and has a wide potential window. Only the anions **3**, **7**, and **28** were examined as PPh_4^+, Me_3NH^+, and Me_4N^+ salts, respectively. An Ag wire was used as a quasi-reference electrode, and ferrocene (Fc) served as an external reference. For all samples studied, plots of the anodic peak current against concentration and against the square root of the scan rate were linear, showing that all electrochemical oxidation reactions are diffusion controlled. Figure 2 presents the voltammograms at a 0.2 V/s scan rate.

An external reference was necessary, since we noticed that in several cases the presence of Fc in the carborane anion solution affects the shape of the voltammogram and shifts the oxidation potentials of both Fc and the carborane. It appears that Fc can act as a homogeneous mediator. In the illustration provided in Figure 3, in the presence of Fc the oxidation peak of the carborane and its counter peak are shifted by several tens of millivolts to lower potentials, the anodic current is doubled, and the Fc peak is slightly affected as well. We now find that the previously reported oxidation potentials of the methylated

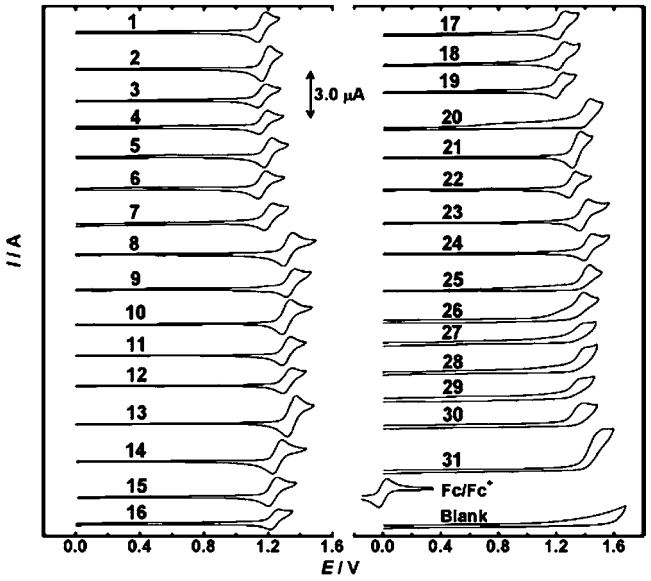

Figure 2. Cyclic voltammograms of (1.0 ± 0.2) × 10^{-3} M salts of carborane anions in liquid SO_2 at 0.2 V/s (0.1 M $NBu_4^+PF_6^-$).

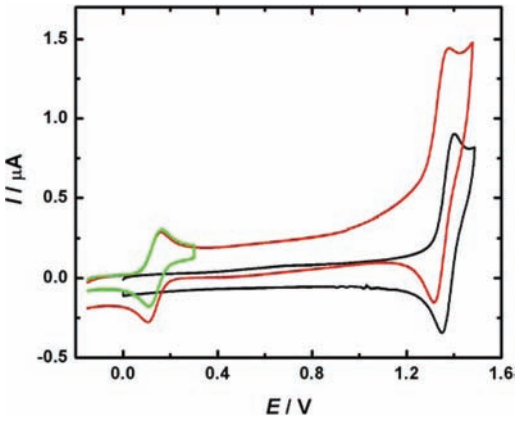

Figure 3. Effect of Fc on the anodic cyclic voltammogram of 0.43 mM **16** in liquid SO_2: (black) **16** alone; (green) Fc alone; (red) **16** and Fc together.

derivatives of the $CB_{11}H_{12}^-$ anion[13,20] were slightly affected by the simultaneous presence of Fc.

Each of the half-wave potentials $E_{1/2}$ (or anodic peak potentials E_{pa} for irreversible systems) and the separation of peak potentials ΔE_p collected in Table 1 is an average of three independent measurements. Not surprisingly, anions differing only in the choice of the alkyl group in position 1 have nearly identical cyclic voltammograms. Almost all the carborane anions exhibit fully chemically reversible one-electron oxidation over the 0.08−5.0 V/s range of scan rates examined, with an approximately 1:1 ratio of anodic and cathodic peak current values. The peak separation ΔE_p is independent of scan rate, and its average value is 0.05 V, similar to that observed for the Fc/Fc^+ couple under the same experimental conditions. The minimal shift of potentials and negligible increase of ΔE_p with increasing scan rate from 80 to 5000 mV/s, along with a cathodic to anodic peak current ratio close to unity, suggest that the neutral radicals are stable in this medium (see Table S1 in the Supporting Information).

The exceptions are the anions **20** (X = COOH, Y = H), which is oxidized reversibly only at scan rates above 1.0 V/s,

dx.doi.org/10.1021/ic2026939 | Inorg. Chem. 2012, 51, 5128−5137

and **25**−**31** (Y = I), whose oxidation is irreversible even at a scan rate of 5.0 V/s, and for which no cathodic counter-peak was observed even in the presence of Fc.

Table 1 also gives calculated reversible oxidation potentials obtained both from the potential energy difference of the anion and the radical at the separately optimized geometry of each ($E_{1/2}^{\Delta E}$) and from the HOMO energy and Koopmans' theorem (E_{aHOMO}). The results were obtained using density functional theory with two common functionals, RI-DFTB3LYP/TZVPP,COSMO and RI-DFTBP86/TZVPP,COSMO, and using Hartree−Fock theory (RI-HF/TZVPP,COSMO). No attempt was made to evaluate frequencies and reaction entropy terms. Absolute calibration was obtained by assuming that the result for **1** is exact. Any other anion could have been used as a reference, but **1** has been studied the most. Calculations were not performed for anions whose position 1 carries an alkyl different from methyl, since the nature of the alkyl group made no difference in the observed electrochemistry.

Figures 4−6 show the plots of the reversible redox potentials against the state energy differences computed with the RI-B3LYP/TZVPP,COSMO, RI-BP86/TZVPP,COSMO, and RI-HF/TZVPP,COSMO methods, respectively.

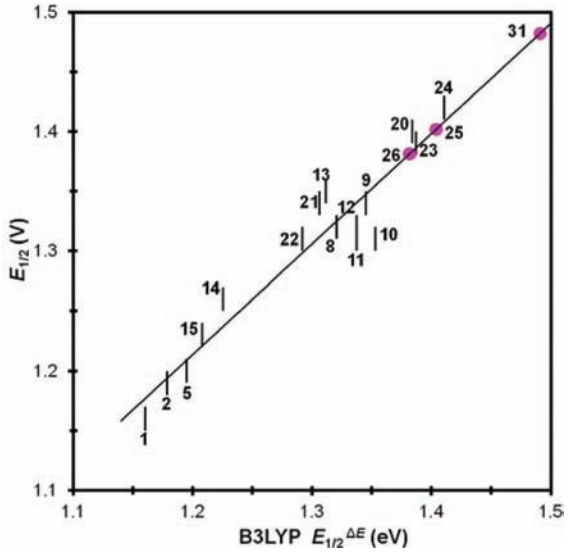

Figure 4. Black bars: measured (y, ±10 mV) vs RI-B3LYP/TZVPP,COSMO state energy difference computed (x) reversible oxidation potentials. Linear regression line: for all reversible data points (y = 0.92x + 0.11, r^2 = 0.92, σ = 0.022 V). Purple circles: reversible oxidation potentials predicted from the regression line.

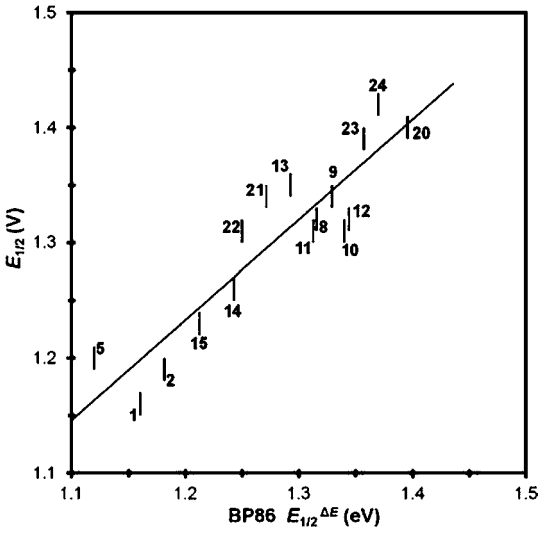

Figure 5. Black bars: measured (y, ±10 mV) vs RI-BP86/TZVPP,COSMO state energy difference computed (x) reversible oxidation potentials. Linear regression line: for all reversible data points (y = 0.87x + 0.19, r^2 = 0.84, σ = 0.032).

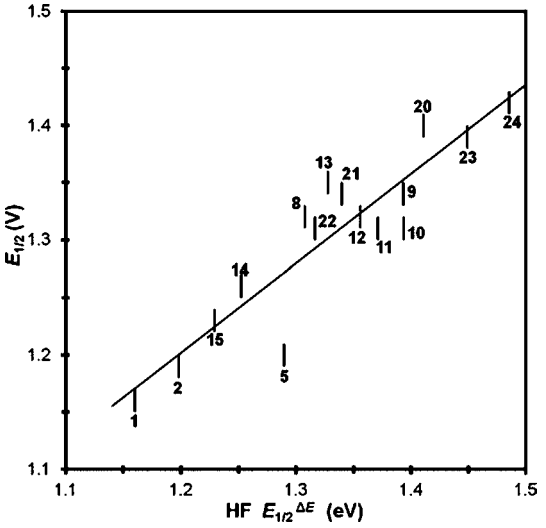

Figure 6. Black bars: measured (y, ±10 mV) vs RI-HF/TZVPP,COSMO state energy difference computed (x) reversible oxidation potentials. Linear regression line: for all reversible data points (y = 0.78x + 0.27, r^2 = 0.84, σ = 0.032).

Correlations based on Koopmans' theorem, in which the redox potentials of the anion are plotted against the HOMO energies of the anion at its optimized geometry, using the RI-B3LYP/TZVPP,COSMO, RI-BP86/TZVPP,COSMO, and RI-HF/TZVPP,COSMO methods, are shown in Figures 7−9, respectively. The calculated geometries of the carborane cage in the anions are all close to 5-fold symmetric and very similar to each other. For example, the B−B distances in the proximate B(2)−B(6) pentagon in all the anions are equal to 1.80 ± 0.01 Å. In contrast, the equilibrium geometries of each radical are quite strongly distorted from 5-fold symmetry and the B−B distance within the B(2)−B(6) pentagon is 1.82 ± 0.07 Å. Within one molecule, the shortest and the longest distances within this pentagon typically differ by 0.1 Å. The details of the distortion vary from radical to radical.

The measured half-wave potentials $E_{1/2}$ (or anodic oxidation potentials E_{pa}) correlated with the Hammett σ_p substituent constants (linear free energy relationship, LFER): $E_{1/2}(R) - E_{1/2}(H) = \rho\sigma_p(R)$ (V).[44,45] Here, either the substituent X in position 1 or the substituent Y in position 12 is held constant and the other is varied, $E_{1/2}(H)$ is the reference value for R = H, and $\sigma_p(R)$ is the Hammett para constant for substituent R (Figure 10). Attempted correlations with other types of substituent constants were poorer. The reaction constants ρ and correlation coefficients r^2 are collected in Table 2.

DISCUSSION

The redox potentials of the four methylated anions that were studied previously (**1**, **2**, **14**, and **15**)[13,20,24] agree well with the reported values. The very minor differences that are observed can be attributed to the previous use of ferrocene internal

dx.doi.org/10.1021/ic2026939 | Inorg. Chem. 2012, 51, 5128−5137

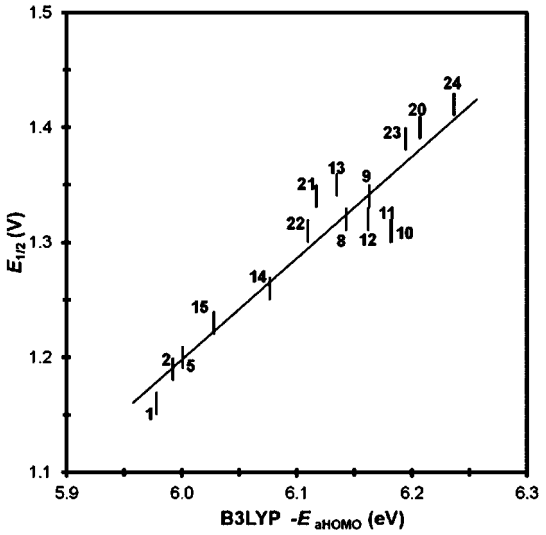

Figure 7. Black bars: measured reversible oxidation potentials (y, ±10 mV) vs RI-B3LYP/TZVPP,COSMO HOMO energy (x) of the anions at their optimized geometries. Linear regression line: for all reversible data points ($y = 0.88x - 4.10$, $r^2 = 0.89$, $\sigma = 0.026$).

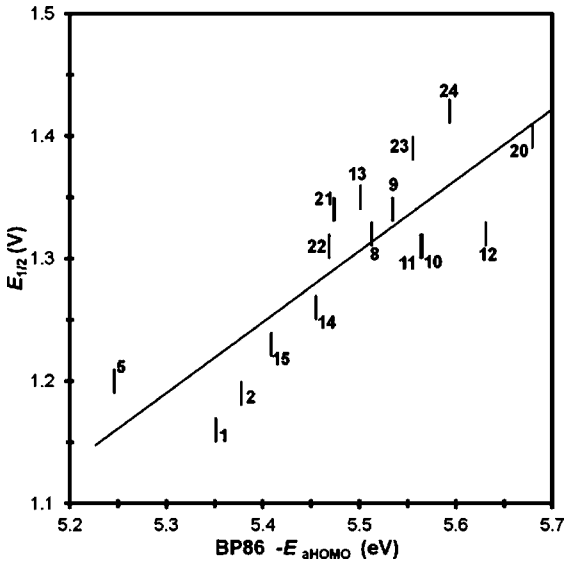

Figure 8. Black bars: measured reversible oxidation potentials (y, ±10 mV) vs RI-BP86/TZVPP,COSMO HOMO energy (x) of the anions at their optimized geometries. Linear regression line: for all reversible data points ($y = 0.58x - 1.88$, $r^2 = 0.71$, $\sigma = 0.043$).

standard and perhaps in part also to the higher temperature used. Since the present data are both more accurate and more numerous than those available previously, they are better suited for an evaluation of substituent effects.

Electrochemical Reversibility. The reversible nature of the electrochemical oxidation of the carborane anions was anticipated from results of previous work,[13,20,24] since they are all sterically encumbered in the antipodal hemisphere, hindering the dimerization of the radical oxidation product. It is likely that many if not all of the reversibly formed neutral radicals could actually be isolated, similarly as $CB_{11}Me_{12}^{\bullet}$,[13] and could be useful as potent neutral oxidants with only weakly nucleophilic reduced forms.[46]

A striking exception is provided by the oxidation of the 12-iodo anions **25**−**31**, which shows no sign of reversibility. At the

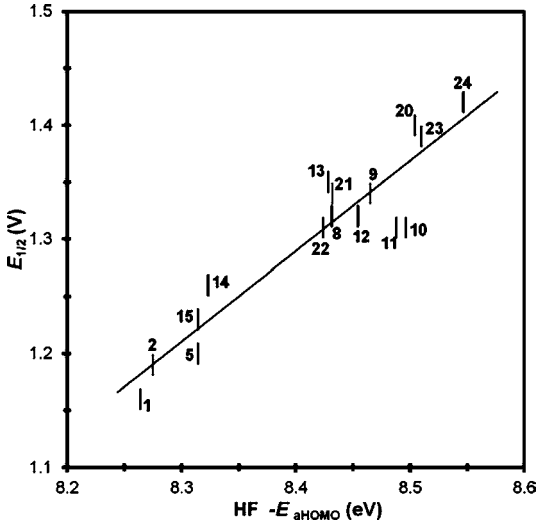

Figure 9. Black bars: measured reversible oxidation potentials (y, ±10 mV) vs RI-HF/TZVPP,COSMO HOMO energy (x) of the anions at their optimized geometries. Linear regression line: for all reversible data points ($y = 0.79x - 5.35$, $r^2 = 0.87$, $\sigma = 0.028$).

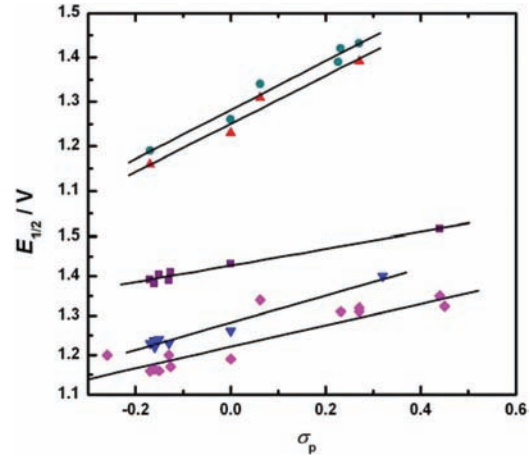

Figure 10. Anodic oxidation potentials $E_{1/2}$ or E_{pa} in liquid SO_2 vs Hammett substituent constant σ_p for varying substituents at X, with Y = Me (pink ◆), H (blue▼) and I (magenta ■) and for varying substituents at Y, with X = Me (red ▲) and H (green ●). Slopes: (pink ◆) $\rho = 0.28$, $r^2 = 0.95$; (blue▼) $\rho = 0.34$, $r^2 = 0.98$; (magenta ■) $\rho = 0.21$, $r^2 = 0.98$; (red ▲) $\rho = 0.54$, $r^2 = 0.98$; (green ●) $\rho = 0.55$, $r^2 = 0.98$.

moment, we can only speculate why this is so. Since the $CB_{11}Me_{12}^{\bullet}$ radical is capable of acting as a methyl radical donor[6,47] in a facile process that leaves behind the neutral borenium ylide $CB_{11}Me_{11}$, it is possible that the relatively weak

Table 2. Comparison of the ρ Values for Different Homologous Series

anion				
X	Y	oxidn	ρ	r^2
varied	H	rev	0.34	0.98
varied	Me	rev	0.28	0.95
H	varied	rev	0.55	0.98
Me	varied	rev	0.54	0.98
varied	I	irr	0.21	0.98

dx.doi.org/10.1021/ic2026939 | Inorg. Chem. 2012, 51, 5128−5137

Scheme 1. Proposed Origin of Irreversibility in the Oxidation of 12-Iodo Anions 25−31

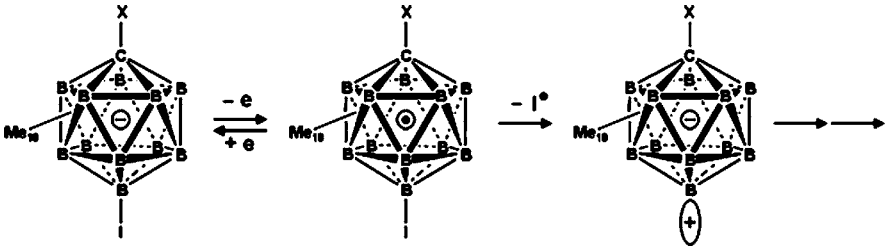

Scheme 2. Proposed Origin of Irreversibility in the Oxidation of the Carboxy Anion 20

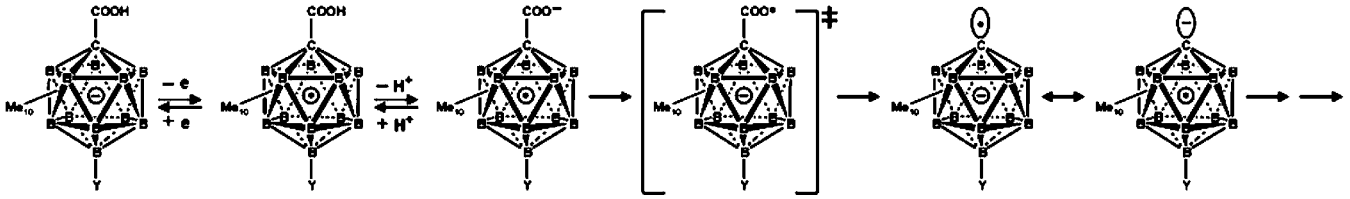

B−I bond in the 12-iodo radicals formed from **25−31** dissociates in a similar fashion by transfer of an iodine atom to the SO_2 solvent to yield highly reactive ylides with a naked vertex in position 12 (Scheme 1), which would then react with one of the nucleophiles present. The cause of the irreversibility is currently under investigation.

The only other anion whose cyclic voltammograms show unmistakable signs of limited reversibility under slow scan conditions is the carboxylic acid **20** (X = COOH, Y = H). In contrast, those of the closely related acid **12** (X = COOH, Y = Me) appear entirely reversible. The oxidized form of **20** clearly has a shorter lifetime due to some destructive process that competes with its back-reduction to the anion. Below we suggest a possible explanation of this surprising difference, but a true resolution of the puzzle can only come from further experiments.

Since the oxidation potential of **20** fits well the Hammett, DFT, and HF correlations and no other oxidation process appears at lower potentials, the primary electrochemical process apparently does not involve an oxidation of the conjugate base, the dianion 1-$^{-}$OCO-12-H-$CB_{11}Me_{10}^{-}$. It is however possible that in the oxidized radical the acidity of the carboxylic group is increased sufficiently for its proton to dissociate, producing the radical anion 1-$^{-}$OCO-12-H-$CB_{11}Me_{10}^{\bullet}$ with unpaired spin density delocalized primarily on the carborane cage, as in other presently studied radicals. Another structure, probably not much higher in energy, is 1-$^{\bullet}$OCO-12-H-$CB_{11}Me_{10}^{-}$, with unpaired spin localized primarily on the carboxy group. This structure differs by an electron transfer from the COO^{-} substituent to the cage. The two structures could be isomers or resonance structures contributing to the description of the electronic structure of a single species. Like most carboxy radicals, this radical anion would be expected to decarboxylate readily and irreversibly (Scheme 2), and we suggest that this could be the cause of electrochemical irreversibility in the oxidation of **20**.

If this explanation is correct, the full reversibility observed with the acid **12** is due to a slower decarboxylation of its radical anion. The 12-methyl substituent would be expected not only to reduce the acidity of the oxidized form of **12** but also to make the transfer of an electron from the COO^{-} substituent to the cage more difficult (cf. the 80 mV difference in the oxidation potentials of **12** and **20**). If the transition state for decarboxylation has increased localization of unpaired spin on the carboxyl group as expected, the activation energy will be increased. Further investigations are under way in an attempt to pinpoint the origin of the irreversible behavior.

Hammett Treatment of Substituent Effects. The traditional treatment of substituent effects is through Hammett correlation with a series of substituent constants, such as the original σ_p or σ_m constants of substituents located on a benzene ring in positions para or meta, respectively, to a functional group. In our case, the carborane cage can be viewed as a somewhat unusual functional group that can be attached to a substituent through several distinct positions, and it is not a priori obvious that any of the known series of Hammett constants will correlate with the observed effect of the substituent on the carborane redox potential. If they did, the slopes of the regression lines would provide information on the relative sensitivity of the various attachment positions to substituent effects.

Somewhat unexpectedly, the present data, limited to attachment positions 1 and 12, actually correlate very well with the substituent σ_p constants (Figure 10, Table 2), with the single exception of the 1-fluoro anion **9**, which is ∼0.1 V harder to oxidize than expected. Interestingly, also the 12-fluoro-substituted anions are slightly harder to oxidize than expected. The slopes ρ of Hammett plots demonstrate that the sensitivity of the anodic oxidation potential of the anions to substituent effects is roughly twice as large in position 12 (slope ∼0.55 V) than in position 1 (∼0.31 V). Correlations with other series of substituent constants are distinctly poorer.

The σ_p constants reflect some mixture of σ (inductive) and π (conjugative) effects of the substituent. The relative importance of these two substituent effects appears to be the same when it comes to affecting the redox potential of the CB_{11} cage or the acidity of a carboxyl in the para position on a benzene ring. Only the electron-withdrawing inductive effect of fluorine on the carborane cage seems to be underestimated relative to its electron-donating conjugative effect, especially when it is located on carbon. The poor correlations with σ_m and σ^+ constants imply that neither the inductive effect nor the conjugative effect alone provides a good description of substituent action.

dx.doi.org/10.1021/ic2026939 | Inorg. Chem. 2012, 51, 5128−5137

Methyl Increments. The expectation from the more limited previous work[20] was that the additive increment for the 1-Me substituent is 52 mV and, for the 12-Me substituent, only 9 mV toward easier oxidation. Both values were small as anticipated, but their relative magnitudes appeared counter-intuitive.[20] The present much more extensive data set shows that the increments based on the reversible potentials alone are 30 mV in position 1 and 68 mV in position 12, and we consider these values reliable. When irreversible redox potentials are included in the evaluation, the increments change only by a few millivolts.

Theoretical Treatment of Substituent Effects. Although the Hammett correlations are instructive, it is interesting to ask whether the observed relative substituent effects on the redox potential can be deduced from first principles. As seen in Figures 4−9, both Hartree−Fock and density functional theory methods achieve this with a standard deviation between 22 and 43 mV when solvent effects are included in the treatment. This is a meaningful accomplishment, considering that the total observed range of values is about 0.25 V (Table 1).

The calculation of potential energy differences between the reduced and oxidized states at the optimized geometry of each is superior to the application of Koopmans' theorem at the equilibrium geometry of the anion, but the difference is surprisingly small. The largest difference between calculated and experimental values is 40, 80, and 90 mV at the B3LYP, BP86, and HF levels, respectively. The best results were obtained with the B3LYP functional, where the slope of the regression line is almost unity (0.92) and the standard deviation σ is 22 mV. With the BP86 functional, the slope is a little lower (0.87) and σ a little higher (32 mV), and in the Hartree−Fock approximation, the slope is only 0.78 and σ = 32 mV. The HF approximation thus underestimates the absolute magnitude of the substituent effects by about 20%. However, it can be used to predict the redox potentials empirically with nearly the same accuracy as the two DFT procedures.

The evaluation of the state energy difference requires two geometry optimizations, with that for the radical being quite difficult. Its results can be compared with those of a simple calculation of HOMO energies at the optimized anion geometry, combined with the use of Koopmans' theorem. While the more complex method produces better results, the improvement is small in the best case of the B3LYP method. Here, Koopmans' theorem yields a regression line slope of 0.88 and σ = 26 mV with a maximum deviation of 50 mV. In the case of the BP86 functional the use of Koopmans' theorem is clearly inferior, as the slope is only 0.58, with σ = 43 mV and a maximum deviation of 140 mV. The combination of the HF method with the Koopmans approximation yields results of intermediate quality, with a slope of 0.79 and σ = 28 mV. Considering the large geometry differences between the anion and radical forms, it is remarkable that the Koopmans' method works as well as it does. For practical purposes, such as a search for anion structures with an optimal redox potential, the combination of a B3LYP calculation with Koopmans theorem promises to be the most cost efficient.

Understanding the Substituent Effects. In addition to providing an opportunity to predict numerical values for the relative effects of substituents on redox potential, quantum chemical methods often also provide an opportunity for achieving their simple intuitive understanding. In the present case, we have not been able to attain this goal. The simplest interpretation of substituent effects on redox potentials is based on a consideration of the Hamiltonian matrix elements (resonance integrals) for the interaction of substituent orbitals with the HOMO of the substrate at the optimized geometry of the anion and use of first-order perturbation theory. In the present case, these elements are negligible, since the HOMO ($4e_2$) has three intersecting nodal planes at both positions of substitution, 1 and 12.[20] However, the substituent effects cover a range of 0.25 V, and the calculated HOMO energies change almost as much.

We suggested previously[13,20] that much of the action of substituents in positions 1 and 12 on the HOMO probably occurs in the strongly distorted neutral radical through their effect on the lower lying HOMO-1 ($5e_1$) with large amplitudes on the tangential p orbitals in these positions, especially on B(12). In the parent $B_{12}H_{12}^{2-}$ structure, the four HOMO and HOMO-1 orbitals are actually degenerate. As a result of the structural distortion, the SOMO of the radical is best described as a mixture of these four orbitals and no longer has nodes going exactly through positions 1 and 12. Unlike the HOMO, the HOMO-1 is expected to respond sensitively to substitution in positions 1 and, particularly, 12. The doubled sensitivity of the redox potential to the substituent effect in position 12 relative to 1 and doubled increment for the methyl substituent support this notion. This description is in qualitative agreement with the amplitudes of the HOMO-1 in these positions in the parent anion $CB_{11}H_{12}^{-}$ [13,20] if it is indeed true that substituents act through the second-order Jahn−Teller mixing of HOMO and HOMO-1 at the distorted radical geometry.

Given the new results reported here, we no longer believe that the substituent effects on the redox potentials can be simply understood in terms of their effect on the energies of Jahn−Teller distorted radicals. At least in the B3LYP calculation, the slope of the regression line that correlates the observed redox potentials with HOMO energies calculated at the anion geometry alone (Figure 7) is not significantly different from that of the line that correlates them with state energy differences, evaluated at anion and radical geometries (Figure 4). Although some fraction of the substituent effect is likely due to Jahn−Teller distortion of the radicals, both to first order due to the degeneracy of the HOMO in the anions and probably also to second order, due to the proximity of their HOMO and HOMO-1, it cannot be decisive.

The present results show that the bulk of substituent effects on the redox potential in positions 1 and 12 is present even at the undistorted anion geometry. We conclude that a simple first-order analysis of the substituent effect on the HOMO energy is not useful. Apparently, one would have to go at least to second order and consider the effect that the interaction of substituent π and σ orbitals with the MOs of the carborane cage has on all of the cage MOs and on the electron distribution in the molecule, which then affects the energies of all the MOs, including the HOMO. As a result, it is understandable why the Hammett analysis leads to the conclusion that both the π and the σ effects of the substituents are important. Perhaps a complex higher order analysis could be cast in simple intuitive terms by taking a suitable point of view, but this task remains for the future.

Finally, we note that the DFT and HF descriptions of the radical at distorted geometries are not likely to be very good, because at the symmetric geometry of the anion the radical has an almost exactly degenerate ground state and requires a description based on two reference functions, and that probably remains true to some diminished degree even at nearby

dx.doi.org/10.1021/ic2026939 | Inorg. Chem. 2012, 51, 5128−5137

distorted geometries. Since a two-reference geometry optimization for systems of this complexity is beyond our current computational capabilities, we refrain from a detailed discussion of the distorted radical geometries and merely note that the presently calculated distortions vary widely from radical to radical. Unfortunately, the reported[13] single-crystal structure of radical **1** is disordered and does not permit a detailed comparison with the calculated equilibrium structures.

SUMMARY

On a platinum electrode in liquid SO_2, icosahedral *closo*-monocarbadodecaborate anions other than those carrying an iodine substituent in position 12 or, to a lesser degree, a carboxy substituent in position 1 exhibit an electrochemically reversible one-electron oxidation behavior even at low scan rates. Mechanistic explanations for the origin of the irreversibility observed in the exceptional cases have been proposed, but further experimentation is necessary to verify them.

The effect of substituents in positions 1 and 12 on the ease of oxidation is larger than might have been expected from the presence of three nodes in the HOMO of the parent C_{5v}-symmetric anionic CB_{11} cluster in these positions. The redox potentials vary linearly with the substituent σ_p Hammett constants, except in the case of 1-fluoro substitution. The observed slopes (reaction constants ρ) show that the susceptibility of position 12 to substituent effects on electrochemical oxidation is double that of position 1. For the methyl group, the corresponding increments are 30 mV in position 1 and 68 mV in position 12. It appears that the substituents in positions 1 and especially 12 act by directly influencing the HOMO-1 of the carborane cluster by their π effect and other MOs of the cluster by their σ effect, and these then transmit the effects to all MOs, including the HOMO, thus affecting the redox potential.

EXPERIMENTAL SECTION

Materials. The carborane salts were prepared and purified by published procedures,[13,20,26,27] except for those of the anions **23** and **24**, whose synthesis is described below. All synthetic manipulations were carried out under an inert atmosphere. THF was dried and distilled from $LiAlH_4$. Liquid ammonia (99%) was purchased from Messer Technogas. $[Me_3NH][CB_{11}H_{12}]$ was purchased from Katchem Ltd. (Elišky Krásnohorské 6, Prague 1, 110 00, Czech Republic). Tetra-*n*-butylammonium hexafluorophosphate obtained from Fluka AG (>98%) was recrystallized twice from ethanol and dried in a vacuum desiccator over P_2O_5. Anhydrous SO_2 gas (99.98%) obtained from Linde Technoplyn, Prague, Czech Republic, was condensed at −65 °C with an ethanol/dry ice bath and purified by stirring magnetically for 30 min in a dried flask with highly activated alumina.

Synthesis. All synthetic procedures used Schlenk inert-atmosphere techniques, and the reaction mixtures were worked up in air. Methyl triflate (Matrix) and sulfolane (Aldrich) were used as purchased. $Cs[12\text{-Br-}CB_{11}H_{11}]$ and $Cs[12\text{-Cl-}CB_{11}H_{11}]$ were synthesized from $[NMe_3H][CB_{11}H_{12}]$ using literature procedures,[48] but we found it necessary to monitor the reactions by ^{11}B NMR spectroscopy to avoid overhalogenation on boron in positions 7−11. NMR was measured with Bruker Avance-III 300 NMR and Varian Inova 500 NMR spectrometers. Peak assignments are based on ^{11}B COSY, $^{1}H-^{11}B$ HETCOR, and continuous wave $^{13}C\{^{11}B\}$ NMR measurements. ^{1}H chemical shifts were measured relative to residual protons from acetonitrile-d_3. ^{11}B chemical shifts were measured relative to $BF_3{\cdot}OEt_2$. Mass spectra were recorded with an electrospray triple quadrupole/time-of-flight mass spectrometer (ESI-qTOF-MS) from Applied Biosystems, PE SCIEX/AB/AP/QSTAR Pulsar Hybrid LC/MS/MS. Elemental analysis was performed by Columbia Analytical Services, Inc.

Cesium 12-Chloro-(2−11)-decamethylcarba-*closo*-dodecaborate, $Cs[1\text{-H-}12\text{-Cl-}CB_{11}Me_{10}]$ (23). A reaction of dried (100 °C, 0.01 Torr, 5 h) $Cs[12\text{-Cl-}CB_{11}H_{11}]$ (1.0 g, 3.22 mmol), CaH_2 (3 g, 71.26 mmol), sulfolane (20 mL) and MeOTf (5 g, 30.47 mmol) was performed and worked up in the way described below for the Cs salt of **24**. The Cs salt of **23** is a white solid (1.17 g, 81% yield). $^{1}H\{^{11}B\}$ NMR (499.8 MHz, CD_3CN): δ −0.32 (s, 15H, B(2−6)-CH_3), −0.13 (s, 15H, B(7−11)-CH_3), 1.22 (s, 1H, CH). $^{1}H\{^{13}C\}\{^{11}B\}$ gHMQC: δ −5.00 (s, B(7−11)-CH_3), −3.45 (s, B(2−6)-CH_3), −58.53 (s, CH). $^{11}B\{^{1}H\}$ NMR (96.2 MHz, CD_3CN): δ −1.23 (s, 1B, B(12)), −9.46 (s, 5B, B(7−11)), −12.82 (s, 5B, B(2−6)). IR (KBr pellet): 2962, 2930, 2896, 2829, 1436, 1307, 1262, 1177, 1099, 1021 cm^{-1}. ESI MS(−): m/z 317, expected isotope distribution. HR ESI MS(−): m/z 317.3217, calcd 317.3226. Anal. Calcd for $CsB_{11}C_{11}H_{31}Br$: C, 29.32; H, 6.93. Found: C, 29.31; H, 7.00.

Cesium 12-Bromo-(2−11)-decamethylcarba-closo-dodecaborate, $Cs[1\text{-H-}12\text{-Br-}CB_{11}Me_{10}]$ (24). Dried (100 °C, 0.01 Torr, 5 h) $Cs[12\text{-Br-}CB_{11}H_{11}]$ (1.0 g, 2.82 mmol) and CaH_2 (3 g, 71.26 mmol) were placed in a two-neck Schlenk round-bottom flask equipped with a stir bar and a septum. The flask was connected to a vacuum line and was evacuated. It was then filled with argon, and sulfolane (20 mL) was syringed in through the septum. The mixture was stirred for 10 min before MeOTf (5 g, 30.47 mmol) was syringed in through the septum. The solution was stirred for 24 h at room temperature and was subsequently heated to 60 °C for 72 h. After this time, ^{11}B NMR and MS/ESI(−) showed complete conversion to product in an aliquot. The flask was allowed to reach room temperature and was opened to air, and dry CH_2Cl_2 (200 mL) was added. The solution was filtered through a coarse frit funnel, and the CaH_2 residue was carefully quenched with isopropyl alcohol and water. Isopropyl alcohol (10 mL) and then water (50 mL) were also added to the filtrate. Finally, excess NH_4OH (50 mL) was added and the solution was stirred for 1 h. Afterward, all volatiles but sulfolane were removed under reduced pressure. Water (100 mL) was added to the sulfolane solution, and a white precipitate formed. CsCl (0.8 g, 4.75 mmol) was added, the solution was filtered, and the white solid was washed with water and dried at 170 °C/0.01 Torr to remove all sulfolane. Recrystallization, first from boiling water and then from benzene, gave analytically pure product as a white solid (1.23 g, 88% yield). $^{1}H\{^{11}B\}$ NMR (499.8 MHz, CD_3CN): δ −0.29 (s, 15H, B(2−6)-CH_3), −0.12 (s, 15H, B(7−11)-CH_3), 1.21 (s, 1H, CH). $^{1}H\{^{13}C\}\{^{11}B\}$ gHMQC: δ −3.97 (s, B(7−11)-CH_3), −3.26 (s, B(2−6)-CH_3), −59.84 (s, CH). $^{11}B\{^{1}H\}$ NMR (96.2 MHz, CD_3CN): δ −1.16 (s, 1B, B(12)), −9.42 (s, 5B, B(7−11)), −12.53 (s, 5B, B(2−6)). IR (KBr pellet): 3019, 2938, 1325, 1221, 1059 cm^{-1}. ESI MS(−): m/z 362, expected isotope distribution. HR ESI MS(−): m/z 362.2706, calcd 362.2705. Anal. Calcd for $CsB_{11}C_{11}H_{31}Br$: C, 26.69; H, 6.31. Found: C, 26.48; H, 6.02.

Electrochemistry. All electrochemical measurements were performed with an AUTOLAB potentiostat (PGSTAT30) controlled by GPES software. The supporting electrolyte was 0.1 M $NBu_4^+PF_6^-$. Experiments were carried out in a single-compartment glass cell using a Pt-disk (1.0 mm diameter) working electrode, a Pt-plate counter electrode, and an Ag rod as quasi-reference electrode as described in the literature.[49] The volume of the five-neck conical shaped electrochemical cell, similar to that used previously,[13,20] was ∼10 mL. The cell with the carborane salt, $NBu_4^+PF_6^-$, and a magnetic stirrer was placed on the vacuum line and heated carefully with a hot air blower for 20 min. Purified SO_2 was distilled into a measuring cell to prepare a sub-millimolar solution (4−5 mL). All cyclic voltammetric measurements were performed at about −65 °C (checked continuously with a thermometer) and at different scan rates from 0.08 to 5.0 V/s. Ferrocene (Fc) was used as an external reference. After the completion of each electrochemical measurement on a carborane, 0.2−0.3 mM Fc was measured in a separate experiment under the same conditions for accurate calibration. Attempts to use Fc as an internal reference were abandoned when it became apparent that it acts as a catalyst or mediator and distorts the results for the

dx.doi.org/10.1021/ic2026939 | Inorg. Chem. 2012, 51, 5128−5137

carborane. The reproducibility of potential measurements was ±10 mV. Anodic (I_{pa}) and cathodic (I_{pc}) peak currents and their ratios at 0.2 V/s are given in the Supporting Information (Table S1).

Calculations. The oxidation potential calculations were performed at the DFT level using the B3LYP[50] and the Becke-Perdew BP86[51,52] functionals and at the Hartree−Fock level with Turbomole 6.1 software.[53] All the calculations were performed using the def2-TZVPP[54] basis set and the RI approximation.[55−57] The geometries of the anions and the neutral radicals were fully optimized at the same level of theory. The solvent effect has been included with the continuum conductor-like screening (COSMO) model.[58,59] The value used for the dielectric constant of liquid SO_2 at −65 °C was 23.7.[60] The resulting B3LYP-optimized geometries and energies of the radicals and anions (Table S2) are given in the Supporting Information. For comparison with the observed redox potentials, a constant was added to all calculated potentials. Its values was chosen so as to obtain a perfect fit for the observed redox potential of **1** relative to the Fc/Fc^+ standard in SO_2.

■ ASSOCIATED CONTENT

Supporting Information

Tables S1 (measured heights of anodic and cathodic peaks) and S2 (DFT computed optimized geometries and energies for anions and radicals) and Figure S1 (vertex numbering in the CB_{11} icosahedron). This material is available free of charge via the Internet at http://pubs.acs.org.

■ AUTHOR INFORMATION

Corresponding Author

*E-mail: jiri.ludvik@jh-inst.cas.cz (J.L.);michl@eefus.colorado.edu (J.M.).

Notes

The authors declare no competing financial interest.

■ ACKNOWLEDGMENTS

We gratefully acknowledge financial assistance from the Ministry of the Education, Youth and Sport of the Czech Republic (LC-510, Z4055905, and KONTAKT ME09002), the Academy of Sciences of the Czech Republic (AV0Z40550506, IAA400550708, and M200550906), the Grant Agency of the Czech Republic (203/09/J058), Universitat de València (UV-INV-AE11-41612), and the US NSF (CHE 0848477), and the Institute of Organic Chemistry and Biochemistry (RVO: 61388963).

■ REFERENCES

(1) Schleyer, P. R.; Najafian, K. *Inorg. Chem.* **1998**, *37*, 3454.
(2) Körbe, S.; Schreiber, P. J.; Michl, J. *Chem. Rev.* **2006**, *106*, 5208.
(3) Reed, C. A. *Acc. Chem. Res.* **1998**, *31*, 133.
(4) Zhang, Y.; Huynh, K.; Manners, I.; Reed, C. A. *Chem. Commun.* **2008**, 494.
(5) Braunecker, W. A.; Akdag, A.; Boon, B. A.; Michl, J. *Macromolecules* **2011**, *44*, 1229.
(6) Volkis, V.; Douvris, C.; Michl, J. *J. Am. Chem. Soc.* **2011**, *133*, 7801.
(7) Janata, M.; Vlček, P.; Látalová, P.; Svitáková, R.; Kaleta, J.; Valášek, M.; Volkis, V.; Michl, J. *J. Polym. Sci. A: Polym. Chem* **2011**, *49*, 2018.
(8) Pospíšil, L.; King, B. T.; Michl, J. *Electrochim. Acta* **1998**, *44*, 103.
(9) Johnson, J. W.; Brody, J. F. *J. Electrochem. Soc.* **1982**, *129*, 2213.
(10) Valášek, M.; Pecka, J.; Jindřich, J.; Calleja, G.; Craig, P. R.; Michl, J. *J. Org. Chem.* **2005**, *70*, 405.
(11) Fanning, J. C. *Coord. Chem. Rev.* **1995**, *140*, 27.
(12) Fete, M. G.; Havlas, Z.; Michl, J. *J. Am. Chem. Soc.* **2011**, *133*, 4123.
(13) King, B. T.; Noll, B. C.; McKinley, A. J.; Michl, J. *J. Am. Chem. Soc.* **1996**, *118*, 10902.
(14) Hawthorne, M. F.; Shelly, K.; Li, F. *Chem. Commun.* **2002**, 547.
(15) Wiersema, R. J.; Hawthorne, M. F. *Inorg. Chem.* **1973**, *12*, 785.
(16) Hawthorne, M. F.; Pilling, R. L.; Stokely, P. F. *J. Am. Chem. Soc.* **1965**, *87*, 1893.
(17) Watson-Clark, R. A.; Knobler, C. B.; Hawthorne, M. F. *Inorg. Chem.* **1996**, *35*, 2963.
(18) Middaugh, R. L.; Farha, F., Jr. *J. Am. Chem. Soc.* **1966**, *88*, 4147.
(19) Wiersema, R. J.; Middaugh, R. L. *J. Am. Chem. Soc.* **1967**, *89*, 5078.
(20) King, B. T.; Körbe, S.; Schreiber, P. J.; Clayton, J.; Němcová, A.; Havlas, Z.; Vyakaranam, K.; Fete, M. G.; Zharov, I.; Ceremuga, J.; Michl, J. *J. Am. Chem. Soc.* **2007**, *129*, 12960.
(21) King, B. T.; Michl, J. *J. Am. Chem. Soc.* **2000**, *122*, 10255.
(22) Bancroft, E. E.; Blount, H. N.; Janzen, E. G. *J. Am. Chem. Soc.* **1979**, *101*, 3692.
(23) Strauss, S. H. *Chem. Rev.* **1993**, *93*, 927.
(24) King, B. T.; Janoušek, Z.; Grüner, B.; Trammel, M.; Noll, B. C.; Michl, J. *J. Am. Chem. Soc.* **1996**, *118*, 3313.
(25) Teixidor, F.; Barbera, G.; Vaca, A.; Kivekäs, R.; Sillanpää, R.; Oliva, J.; Viñas, C. *J. Am. Chem. Soc.* **2005**, *127*, 10158.
(26) Valášek, M.; Štursa, J.; Pohl, R.; Michl, J. *Inorg. Chem.* **2010**, *49*, 10247.
(27) Valášek, M.; Štursa, J.; Pohl, R.; Michl, J. *Inorg. Chem.* **2010**, *49*, 10255.
(28) Moens, J.; Jaque, P.; De Proft, F.; Geerlings, P. *J. Phys. Chem. A* **2008**, *112*, 6028.
(29) Winget, P.; Weber, E. J.; Cramer, C. J.; Truhlar, D. G. *Theor. Chem. Acc.* **2004**, *112*, 217.
(30) Li, J.; Fisher, C. L.; Chen, J.; Bashford, D.; Noodleman, L. *Inorg. Chem.* **1996**, *35*, 4694.
(31) Uudsemaa, M.; Tamm, T. *J. Phys. Chem. A* **2003**, *107*, 9997.
(32) Jacque, P.; Marenich, A. V.; Cramer, C. J.; Truhlar, D. G. *J. Phys. Chem. C* **2007**, *111*, 5783.
(33) Roy, L. E.; Jakubikova, E.; Guthrie, M. G.; Batista, E. R. *J. Phys. Chem. A* **2009**, *113*, 6745.
(34) Quiñonero, D.; Kaledin, A. L.; Kuznetsov, E.; Geletii, Y. V.; Besson, C.; Hill, C. L.; Musaev, D. G. *J. Phys. Chem. A* **2010**, *114*, 535.
(35) Charles-Nicolas, O.; LaCroix, J. C.; Lacaze, P. C. *J. Chim. Phys.* **1998**, *95*, 1457.
(36) Winget, P.; Weber, E. J.; Cramer, C. J.; Truhlar, D. G. *Phys. Chem. Chem. Phys.* **2000**, *2*, 1231.
(37) Phillips, K. L.; Sandler, S. I.; Chiu, P. C. *J. Comput. Chem.* **2011**, *32*, 226.
(38) Baik, M.-H.; Friesner, R. A. *J. Phys. Chem. A* **2002**, *106*, 7407.
(39) Nafady, A.; Costa, P. J.; Calhorda, M. J.; Geiger, W. E. *J. Am. Chem. Soc.* **2006**, *128*, 16587.
(40) Follet, A. D.; McNabb, K. A.; Peterson, A. A.; Scanlon, J. D.; Cramer, C. J.; McNeill, K. *Inorg. Chem.* **2007**, *46*, 1645.
(41) Wang, H. J.; Yu, C. J. *Res. Chem. Intermed.* **2010**, *36*, 1003.
(42) Kuhn, A.; von Eschwege, K. G.; Conradie, J. *Electrochim. Acta* **2011**, *56*, 6211.
(43) Haya, L.; Sayago, F. J.; Mainar, A. M.; Cativiela, C.; Urieta, J. S. *Phys. Chem. Chem. Phys.* **2011**, *13*, 17696.
(44) Zuman, P. *Substituent Effects in Organic Polarography*; Plenum: New York, 1967; p 46.
(45) Jaffe, H. H. *Chem. Rev.* **1953**, *53*, 191.
(46) Zharov, I.; Weng, T.; Orendt, A. M.; Barich, D. H.; Penner-Hahn, J.; Grant, D. M.; Havlas, Z.; Michl, J. *J. Am. Chem. Soc.* **2004**, *126*, 12033.
(47) Zharov, I.; Havlas, Z.; Orendt, A. M.; Barich, D. H.; Grant, D. M.; Fete, M. G.; Michl, J. *J. Am. Chem. Soc.* **2006**, *128*, 6089.
(48) Jelinek, T.; Baldwin, P.; Scheidt, W. K.; Reed, C. A. *Inorg. Chem.* **1993**, *32*, 1982.
(49) Ceroni, P.; Paolucci, F.; Paradisi, C.; Juris, A.; Roffia, S.; Serroni, S.; Campagna, S.; Bard, A. J. *J. Am. Chem. Soc.* **1998**, *120*, 5480.
(50) Becke, A. D. *J. Chem. Phys.* **1993**, *98*, 5648.
(51) Becke, A. D. *Phys. Rev. A* **1988**, *38*, 3098.

(52) Perdew, J. P. *Phys. Rev. B* **1986**, *33*, 8822.
(53) Ahlrichs, R.; Bär, M.; Häser, M.; Horn, H.; Kölmel, C. *Chem. Phys. Lett.* **1989**, *162*, 165.
(54) Weigend, F.; Furche, F.; Ahlrichs, R. *J. Chem. Phys.* **2003**, *119*, 12753.
(55) Eichkorn, K.; Treutler, O.; Öhm, H.; Häser, M.; Ahlrichs, R. *Chem. Phys. Lett.* **1995**, *242*, 652.
(56) Eichkorn, K.; Weigend, F.; Treutler, O.; Ahlrichs, R. *Theor. Chem. Acc.* **1997**, *97*, 119.
(57) Weigend, F. *Phys. Chem. Chem. Phys.* **2006**, *8*, 1057.
(58) Klamt, A.; Schuurmann, G. *J. Chem. Soc., Perkin Trans. 2* **1993**, *2*, 799.
(59) Schäfer, A.; Klamt, A.; Sattel, D.; Lohrenz, J. C. W.; Eckert, F. *Phys. Chem. Chem. Phys.* **2000**, *2*, 2187.
(60) Lichtin, N. N.; Wasserman, B.; Reardon, J. F. *J. Phys. Chem.* **1981**, *85*, 1590.

dx.doi.org/10.1021/ic2026939 | *Inorg. Chem.* 2012, 51, 5128−5137